Submitted to small NANO MICRO

DOI: 10.1002/smll.((please add manuscript number))

# Structural Reinforcement of Microvascular Networks Using Electrostatic Layer-by-Layer Assembly with Halloysite Nanotubes**

*Solar C. Olugebefola, Andrew R. Hamilton, Daniel J. Fairfield, Nancy R. Sottos, and Scott R. White**

*((Optional Dedication))*

[*] Prof. A. B. Corresponding-Author, Dr. C. Author-Two
Address line 1
Address line 2, postcode (Country)
E-mail: ((insert))
Dr. D. E. F. Author-Three
Address line 1
Address line 2, postcode (Country)

((Acknowledgements, general annotations, funding.))

Supporting Information is available on the WWW under http://www.small-journal.com or from the author.

Keywords: ((Five maximum))

The evolution of two-dimensional microfluidic devices into three dimensions has expanded the utility of microchannel networks into the regime of structural materials. Epoxy matrices containing integrated networks filled with active fluids have demonstrated the ability to indicate internal damage[1-4] as well as to autonomously heal from single[4-6] and repeated[5,7,8] damage events. In this respect, these systems bear a significant resemblance to natural vasculature, which functions to transport fluids throughout biological tissue for various functions including, but not limited to self-healing. We seek to create structures that couple this added functionality with robust structural behavior through the introduction of reinforcing particles at channel interior surfaces.

Currently there are several prominent methods for creating networks in polymer or polymer-composite matrices, including laser ablation,[9-13] and stereolithographic polymerization.[14] In the area of self-healing polymer networks, the two most documented fabrication techniques are hollow fiber embedment and the use of sacrificial scaffolds. Embedment consists of replacing solid glass fibers in a composite ply with hollow glass fibers capable of carrying active fluids.[1,15-22] This method has the advantage of facile incorporation into a widely used and well-characterized glass fiber composite fabrication process. However, materials with these incorporated fibers are restricted to channels that are isolated from each other and run uniaxially within each ply in order to align with the surrounding load-bearing fibers. In contrast, scaffold-based networks are formed by the fabrication of an arbitrarily shaped template from a fugitive material that is then surrounded with an epoxy matrix, and removed, leaving a series of interconnected hollow channels.[7,8,23-26] Our research group has studied networks made using direct-write assembly, in which a hydrocarbon microcrystalline wax is extruded to form the scaffold using robotically controlled deposition.[27] With appropriate methods of scaffold fabrication, the advantage of this second

method is greater control over network design as channels can have non-linear shapes and linkages, but due to the absence of load-bearing glass fibers these materials experience a reduction in bulk mechanical properties. When subjected to high loads, unreinforced microchannels can provide paths for crack propagation and act as strain concentrators leading to microcrack nucleation.

Within stiffer vascular biological tissues such as dentin (found in teeth) and bone, similar mechanical deficiencies are mitigated by the presence of complex hierarchical structural features near to channel surfaces. Dentin contains oriented microscale tubules 1-2 μm in diameter running through the length of the tissue. A region of high mineralization and correspondingly high stiffness surrounds each tubule[28] and these regions increase material toughness by forming energy-absorbing microcracks and deflecting larger cracks from their lowest energy paths.[29,30] Haversian canals used to transport nutrients in osteonal bone are another example of biological vasculature in hard materials. These canals are surrounded by a complex lamellar hybrid of hydroxyapatite and collagen fibrils.[31,32] Mechanically this results in a stiffness profile that oscillates radially near the canal, that functions to arrest impinging cracks[33] and reduce microcrack initiation at canal surfaces.

Modifying the local mechanical properties in a synthetic microvascular material near channel surfaces would enhance the overall properties of the matrix and increase the viability of microvascular networks for practical application. Using direct-write assembly, Therriault et al. have fabricated templates using robotic deposition of a fugitive microcrystalline wax in order to make self-healing microvascular materials.[27] Preliminary research suggests that these scaffold-based networks are strengthened by the addition of an alumina microparticle layer to the surface of the scaffold before prepolymer infiltration, thus transferring reinforcing layer onto the epoxy network channel walls. Fluorescence-based digital image correlation (FDIC) measurements of single channels in cross-section have shown a significant reduction in strain concentrations around surface-modified channels suggesting increased stress tolerance.[26]

FDIC is a relatively new extension of the digital image correlation technique and has been used to measure real time, full field strains on the microscale with nanoscale resolution for polymers under load with both interior[34-36] and surface[26] micron-scale inhomogeneities. The technique is ideal for microvascular systems, allowing the direct measurement of the field local to embedded channels. To measure two-dimensional strains, fluorescent polymeric nanoparticles are deposited onto a sample surface to produce a random optical pattern. By imaging the pattern before and during loading, and matching small subsets of images from the normal and deformed states, an optimized correlation coefficient is determined for the local displacement vectors $u$ and $v$ and the displacement gradients $\partial u/\partial x$, $\partial u/\partial y$, $\partial v/\partial x$, $\partial v/\partial y$.[37] Regardless of magnification, the technique is accurate to ± 0.1 pixels in displacement as long as a sufficiently distinguishable pattern can be generated.

To more systematically determine the effects of particle-containing reinforcement layers on the mechanical properties of embedded networks we use electrostatic layer-by-layer assembly (ELbL) to deposit films containing oxide nanoparticles onto scaffold surfaces before matrix infiltration, leading to embedded-particle regions at the resultant channel surface. We then examine the changes in strain concentration versus increases in reinforcing region thickness for the resultant network. ELbL is a well-developed technique for depositing polyelectrolytes and charged particles onto substrates with nanoscale control over layer thickness and chemical composition. Films are built through the alternating immersion of a substrate into aqueous solutions of oppositely charged components leading to incremental buildup of surface films.[38-40] Due to the solution-based nature of the deposition, films can be conformally built onto non-planar substrates, a necessary aspect of modifying three-dimensional scaffolds. The technique is extremely versatile, used to make polymer/polymer, polymer/nanoparticle, and nanoparticle/nanoparticle films. Lvov and coworkers have

demonstrated the assembly of halloysite and the polycation poly(diallyldimethyl ammonium) chloride (PDADMAC) onto planar glass substrates with reasonable uniformity.[41] Halloysite is a naturally occurring aluminosilicate nanotube [42] with a net negative surface charge, used as a toughening agent in thermoset epoxies.[43-45] Here we seek to use the halloysite/PDADMAC multilayer system to modify the channel structure of scaffold-assembled microvascular network materials by depositing directly onto network template surfaces and thereby transferring the particles to the subsequent matrix.

Adapting halloysite multilayer assembly to fugitive wax scaffolds requires consideration of a number of elements. To enable ELbL assembly, the standard hydrocarbon-rich fugitive wax ink was modified to carry a negative surface charge through the addition of stearic acid. Inks with too high a proportion of the additive demonstrated degraded rheological behavior making scaffold writing extremely difficult. Usable writing formulations contained up to 10 wt% stearic acid, though more ideal writing speeds were achieved with ~5 wt% which was used for almost all sample fabrication. Scaffolds with beam diameters of 200 μm were written atop glass slides or silicone molds for support during the multilayer deposition process. Flat wax samples on glass slides were also treated in the multilayer deposition process in order to be characterized by scanning electron microscopy (SEM). The ELbL process consists of immersion in a $10^{-2}$ M aqueous PDADMAC solution followed by water rinsing, then immersion into an aqueous dispersion of 1 g $L^{-1}$ halloysite and further water rinsing. The halloysite was dispersed in solution through ultrasonication and the quality of the dispersion was characterized by dynamic light scattering. The average particle diameter of halloysite in solution was determined to be 153 nm, which suggests single nanotubes without significant quantities of clusters present. Multilayers were assembled by cycling the immersion process repeatedly to yield films denoted by $(\text{PDADMAC/halloysite})_n$ where $n$ is the number of polymer-halloysite bilayers.

An SEM image of a $(\text{PDADMAC/halloysite})_{20}$ film deposited onto a wax surface is shown in **Figure 1a**. Nanotubes can be clearly discerned on the surface within the PDADMAC binding polymer, completely covering the wax surface. Electron dispersive x-ray spectroscopy confirmed the presence of aluminum, silicon, oxygen and carbon consistent with the presences of halloysite, wax and polymer (See Supporting Information). In order to assess the overall coverage of the multilayer film on fabricated scaffolds, we imaged samples with microscale computed x-ray tomography (MicroCT). Figure 1b shows a representative 3-dimensional reconstruction of a scaffold section with a deposited 80 bilayer film where the brightness is correlated to x-ray contrast. The film demonstrably reaches all locations on the scaffold, including high curvature regions where wax beams intersect. The voxel resolution of the instrument is limited to approximately 1 $\mu m^2$ when examining a full network and thinner layer regions manifest as gaps in the high contrast coating while thicker regions appear as bright spots.

After multilayer assembly, scaffolds were surface functionalized with a glycidyl silane to promote epoxy adhesion then infiltrated with a liquid epoxy prepolymer and cured. Scaffolds were removed by a combination of heating and chemical solvation leaving hollow channels within the matrix. To determine the efficacy of transfer of the mutilayer to the epoxy surface, fractured network specimens were examined at channel intersections. An SEM image of a representative region between two channels shows the narrowing edge of epoxy before they meet Figure 1c. The presence of halloysite is evident to a gap size of approximately 1-2 μm demonstrating the conformal nature of the deposition. Due to the fragility of the scaffold, measuring multilayer thickness directly from deposition was infeasible. Instead, we fabricated single channel samples and then fractured them to reveal axial cross-sections. **Figure 2** shows channel edges of samples with increasing numbers of bilayers embedded in the epoxy matrix. The lack of visible interface between the epoxy and

the multilayers is evidence of favorable bonding. From these images, the thickness is correlated to the number of bilayers deposited (See Supporting Information). As suggested by the MicroCT measurements of the scaffold, the thickness variation increases significantly with the number of bilayers. The multilayer assembly process exhibits linear thickness growth with a per-bilayer thickness of approximately 188 nm, which is only slightly larger than the average halloysite tubule diameter measured by light scattering. This value suggests monolayer or near-monolayer deposition per cycle. The variation in multilayer thickness is evident from MicroCT scans of an 80-bilayer reinforced network after scaffold removal (Supporting Information).

To determine the effects of increasing layer thickness on mechanical properties, we performed FDIC measurements on samples with single channels under uniaxial tension normal to the channel axis. Images taken before and during loading were correlated to yield a displacement field along with corresponding displacement gradient fields. To act as a control, far-field strains were first measured in flat regions of each sample free of surface features, and strain uniformity was confirmed by a standard deviation over the image field of less than 5 percent. **Figure 3a** shows the normalized $\varepsilon_{xx}$ strain fields near to channels (blanked out) both unreinforced and with (PDADMAC/Halloysite) multilayers embedded. In these images, the loads are applied horizontally and the maximum strains are located directly above and below the channels while the minimum strains are located along the loading axis. Compared to the control sample the presence of the multilayer suppresses the amplitude of these maximum strains. The effect of 20-bilayers is less pronounced than that for 40- and 80-bilayers. In the latter cases the strain along the vertical axis drops below that of the far-field strain further from the channel ($\varepsilon_{xx} < 1$) suggesting a significant reinforcing effect. A histogram of strain values above and below the channel clearly illustrates the decrease in strain with increasing halloysite layer thickness (Figure 3b). At 80-bilayers, the mode of the strain field – taken as the peak of the histogram – transitions below that of the far-field strain, though there is still an observable stress concentration near to the channel edge.

In order to estimate the elastic modulus of the reinforcing material, we compared strain fields for 80-bilayer samples to analytical solutions for channels with a reinforced interlayer ring in an infinite plate.[46] The multilayer thickness measured by SEM and channel diameter measured by optical imaging were used as inputs to yield analytical solutions that reasonably matched the FDIC strain field when the ring modulus was estimated to be 10 GPa. Using this modulus value to simulate strain fields for 40- and 20-bilayer samples also matched experimental results (Supporting Information). This value is significantly lower than bulk values for alumina or silica, and more than an order of magnitude lower than theoretically modeled values for single halloysite nanotubes, which are in the range of 234-339 GPa.[47] The reduced modulus is likely due to two factors. The first is weak bonding between the halloysite and the PDADMAC within the multilayer, which is ionic rather than covalent. Secondly, the introduction of halloysite particles to bulk epoxy has been shown to significantly increase toughness, but the effects on modulus have been less pronounced.[43,45] Ideally, strengthening the reinforcement layer would involve increasing the relative ratio of oxide to polymer, which may be possible by increasing the particle size, or by changing the polymer and particle charge densities in solution to control the degree of deposition of each component per layer.

In summary, the electrostatic layer-by-layer assembly technique can be used to controllably deposit halloysite nanotubes onto channel surface interiors in microvascular networks. The deposition is facile for reasonably complex microscale features, limited by the size of the depositing particles. Halloysite acts as a local structural reinforcing agent at appropriate thicknesses and bonds readily to epoxy matrix materials. By reducing the stress concentration near to microchannels, the multilayer should improve the matrix mechanical

properties and therefore the robustness of these networks to physical damage. The ELbL technique should be applicable to deposition of other types of oxide nano- and microparticles, which may demonstrate even stronger reinforcing effects depending on particle shape and size.

## Experimental Section

*Materials*: Fugitive wax ink was made from mixtures of mineral oil (Fisher Scientific), microcrystalline wax (Strahl & Pitsch Inc.) and stearic acid (Sigma-Aldrich) in either a 43:57:5 or a 43:57:10 w/w/w ratio. Epoxy was composed of EPON 828:Epikure 3274 (Miller-Stephenson) combined in a 5:2 w/w ratio. Poly(diallyldimethyl ammonium chloride) and halloysite nanoclay were received from Aldrich. Z-6040 glycidoxysilane was received from Dow Corning.

*Scaffold preparation*: Fugitive scaffolds were assembled by the direct-write process as detailed by Therriault et al.[27] Ink loaded into pressurized syringes was pattern-deposited onto substrates using a robotic positioning platform (Aerotek) building a planar line pattern, then building a second layer above that and repeating to yield a three-dimensional scaffold. Multilayers were assembled onto scaffolds by alternating immersion in aqueous solutions/dispersions of $10^{-2}$ M PDADMAC and 1mg/mL halloysite with three intermediate Milli-Q pure rinse baths in a Stratosequence6 (Nanostrata, Inc.) dipper. Halloysite dispersions were pH adjusted to 8.5 or higher to insure negative particle surface charge and ultrasonicated for 5 minutes prior to deposition.

*Epoxy sample preparation*: Scaffolds were immersed in a 0.5 v/v% aqueous solution of Z-6040 at pH 4.5 for 15 minutes to promote better adhesion to epoxy precursors, then infiltrated with mixed epoxy pre-polymer and allowed to solidify overnight at room temperature, followed by a 3-day cure at 30º C. Finished polymer parts were heated above the wax melting temperature in order to wick out scaffold materials, followed by room temperature immersion in petroleum ether to remove any hydrocarbon residue. MicroCT samples were imaged after curing with no modification. Samples examined by SEM were fractured to obtain axial cross-sections then sputter-coated with gold-palladium to enhance imaging quality. Samples measured by FDIC were cut to reveal radial cross-sections with an Isomet 1000 saw (Buehler), then surface polished using a Buehler Ecomet 3 in several stages down to 4000 grit to obtain a flat surface and coated with ~300 nm diameter silica particles containing the fluorescent dye rhodamine B to generate a correlation pattern.

*Characterization*: Light-scattering measurements of halloysite dispersions < 0.1 g $L^{-1}$ were carried out using a NICOMP 380 ZLS particle sizer (Particle Sizing Systems). SEM images and EDS spectra were obtained with a Philips XL30 ESEM-FEG with EDAX attachment. MicroCT was performed using an Xradia MicroXCT-200.

*FDIC:* Samples were imaged using a Leica DM-R fluorescence microscope with a 10x objective lens and 1280x1024 pixel resolution Qimaging Retiga 1300 digital camera. Image resolution was determined to be 534 nm per pixel. Correlations were performed with custom DIC code where a course-fine search is used to obtain an initial guess for a Newton-Raphson scheme [37]. Subset sizes were 16.5 by 16.5 μm and correlations were performed every 5.3 μm. Samples were imaged, then loaded in uniaxial tension using a load frame (Ernest F. Fullam, Inc.) and imaged a second time under load. Applied load was measured using a 100 lb.

capacity load cell (Entran) and loading rate was kept constant at 1 μm/s. After unloading, samples were allowed to relax for 30 minutes between measurements.


(1) Bleay, S. M.; Loader, C. B.; Hawyes, V. J.; Humberstone, L.; Curtis, P. T. *Composites Part A: Applied Science and Manufacturing* **2001**, *32*, 1767–1776.
(2) Pang, J. W. C.; Bond, I. P. *Composites Part A: Applied Science and Manufacturing* **2005**, *36*, 183-88.
(3) Pang, J. W. C.; Bond, I. P. *Composites Science And Technology* **2005**, *65*, 1791-99.
(4) Trask, R.; Bond, I. *Smart Materials and Structures* **2006**, *15*, 704-10.
(5) Toohey, K. S.; Sottos, N. R.; Lewis, J. A.; Moore, J. S.; White, S. R. *Nat Mater* **2007**, *6*, 581-85.
(6) Trask, R. S.; Williams, G. J.; Bond, I. P. *Journal of the Royal Society Interface* **2007**, *4*, 363-71.
(7) Toohey, K. S.; Hansen, C. J.; Lewis, J. A.; White, S. R.; Sottos, N. R. *Advanced Functional Materials* **2009**, *19*, 1399-405.
(8) Hansen, C. J.; Wu, W.; Toohey, K. S.; Sottos, N. R.; White, S. R.; Lewis, J. A. *Advanced Materials* **2009**, *21*, 4143-47.
(9) Yoshida, Y. In *Fourth International Symposium on Laser Precision Microfabrication, 21-24 June 2003*; Proc. SPIE - Int. Soc. Opt. Eng. (USA); SPIE-Int. Soc. Opt. Eng: USA, 2003; Vol. 5063, pp. 189-92.
(10) Saxena, I.; Agrawal, A.; Joshi, S. *Journal of Micromechanics and Microengineering* **2009**, *19*.
(11) Rizvi, N. In *Design, Test, and Microfabrication of MEMS and MOEMS, 30 March-1 April 1999*; Proc. SPIE - Int. Soc. Opt. Eng. (USA); SPIE-Int. Soc. Opt. Eng: USA, 1999; Vol. 3680, pp. 546-52.
(12) Hayden, C. *Journal of Micromechanics and Microengineering* **2003**, *13*, 599-603.
(13) Heng Qi; Tao Chen; Liying Yao; Tiechuan Zuo *Optics and Lasers in Engineering* **2009**, *47*, 594-8.
(14) Kang, H.; Lee, I. H.; Cho, D. *J. Manuf. Sci. Eng.* **2004**, *126*, 766.
(15) Pang, J. W. C.; Bond, I. P. *Composites Part A* **2005**, *36*, 183–188.
(16) Pang, J. W. C.; Bond, I. P. *Composites Science and Technology* **2005**, *65*, 1791-1799.
(17) Trask, R. S.; Bond, I. P. *Smart Materials and Structures* **2006**, *15*, 704-710.
(18) Williams, H. R.; Trask, R. S.; Bond, I. P. *SMART MATERIALS & STRUCTURES* **2007**, *16*, 1198-1207.
(19) Bond, I. P.; Trask, R. S.; Williams, H. R. *MRS BULLETIN* **2008**, *33*, 770-774.
(20) Williams, H. R.; Trask, R. S.; Bond, I. P. *COMPOSITES SCIENCE AND TECHNOLOGY* **2008**, *68*, 3171-3177.
(21) Kousourakis, A.; Mouritz, A. P.; Bannister, M. K. *Composite Structures* **2006**, *75*, 610–618.
(22) Kousourakis, A.; Bannister, M. K.; Mouritz, A. P. *Composites Part A* **2008**, *39*, 1394–1403.
(23) Bellan, L. M.; Singh, S. P.; Henderson, P. W.; Porri, T. J.; Craighead, H. G.; Spector, J. A. *Soft Matter* **2009**, *5*, 1354.
(24) Toohey, K. S.; Sottos, N. R.; Lewis, J. A.; Moore, J. S.; White, S. R. *NATURE MATERIALS* **2007**, *6*, 581-585.
(25) Toohey, K. S.; Sottos, N. R.; White, S. R. *Experimental Mechanics* **2009**, *49*, 707-17.
(26) Hamilton, A.; Sottos, N.; White, S. *Experimental Mechanics* **2010**, *50*, 255-263.
(27) Therriault, D.; White, S.; Lewis, J. *Nature Materials* **2003**, *2*, 265-271.
(28) Balooch, G.; Marshall, G. W.; Marshall, S. J.; Warren, O. L.; Asif, S. A. S.; Balooch, M. *Journal of Biomechanics* **2004**, *37*, 1223–1232.
(29) Nalla, R. K.; Kinney, J. H.; Ritchie, R. O. *Journal of Biomedical Materials Research* **2003**, *67*, 484–495.

(30) Nalla, R. K.; Kinney, J. H.; Ritchie, R. O. *Biomaterials* **2003**, *24*, 3955–3968.
(31) Black, J.; Mattson, R.; Korostoff, E. *Haversian Osteons: Size, Distribution, Internal Structure and Orientation.*; United States, 1974; p. 12p.
(32) Evans, F.; Vincentelli, R. *Journal of Biomechanics* **1974**, *7*, 1-10.
(33) Gupta, H.; Stachewicz, U.; Wagermaier, W.; Roschger, P.; Wagner, H.; Fratzl, P. *Journal of Materials Research* **2006**, *21*, 1913-1921.
(34) Berfield, T.; Patel, J.; Shimmin, R.; Braun, P.; Lambros, J.; Sottos, N. *Small* **2006**, *2*, 631-5.
(35) Franck, C.; Hong, S.; Ravichandran, G.; Maskarinec, S.; Tirrell, D. *Experimental Mechanics* **2007**, *47*, 427-38.
(36) Samuel, B.; Demirel, M.; Haque, A. *JOURNAL OF MICROMECHANICS AND MICROENGINEERING* **2007**, *17*, 2324-2327.
(37) Bruck, H.; McNeill, S.; Sutton, M.; Peters, W. *Experimental Mechanics* **1989**, *29*, 261-7.
(38) Decher, G.; Hong, J. *European Conference on Organized Organic Thin Films* **1991**, 321.
(39) Decher, G.; Hong, J. *Berichte der Bunsengesellschaft fuer Physikalische Chemie* **1991**, *95*, 1430.
(40) Decher, G. In *Multilayer Thin Films: Sequential Assembly of Nanocomposite Materials*; Decher, G.; Schlenoff, J. B., Eds.; Wiley-VCH: Weinheim, Germany, 2003; Vol. 1, pp. 1-46.
(41) Lvov, Y.; Price, R.; Gaber, B.; Ichinose, I. Colloids and Surfaces A: Physicochemical and Engineering Aspects; Elsevier, 2002; Vol. 198-200, pp. 375-382.
(42) Joussein, E.; Petit, S.; Churchman, J.; Theng, B.; Righi, D.; Delvaux, B. *Clay Minerals* **2005**, *40*, 383-426.
(43) Liu, M.; Guo, B.; Du, M.; Cai, X.; Jia, D. *Nanotechnology* **2007**, *18*, 455703.
(44) Ye, Y.; Chen, H.; Wu, J.; Ye, L. *Polymer* **2007**, *48*, 6426–6433.
(45) Deng, S.; Zhang, J.; Ye, L.; Wu, J. *Polymer* **2008**, *49*, 5119–5127.
(46) Savin, G. N. *Stress concentration around holes.*; New York,, 1961.
(47) Guimaraes, L.; Enyashin, A. N.; Seifert, G.; Duarte, H. A. *Journal of Physical Chemistry C* **2010**, *114*, 11358-11363.

Received: ((will be filled in by the editorial staff))
Revised: ((will be filled in by the editorial staff))
Published online on ((will be filled in by the editorial staff))

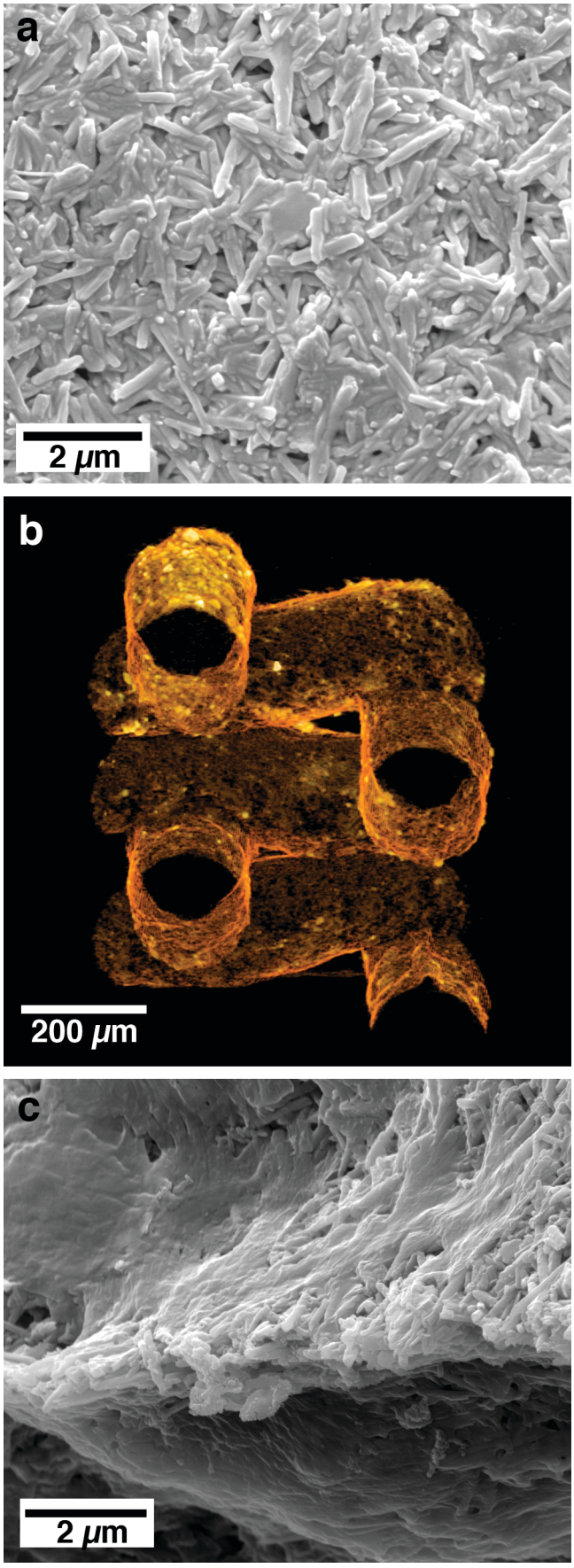


**Figure 1.** a) SEM image of PDADMAC/halloysite multilayer deposited onto flat wax surface showing isotropic nanotube orientation. b) MicroCT reconstruction of

(PDADMAC/halloysite)$_{80}$ multilayer deposited onto fugitive network scaffold. Multilayer coverage reaches all locations on the scaffold surface. c) SEM image of epoxy matrix with embedded PDADMAC/halloysite multilayer at the intersection between two channels. The minimum radius of curvature for the deposited halloysite is less than 2 μm.

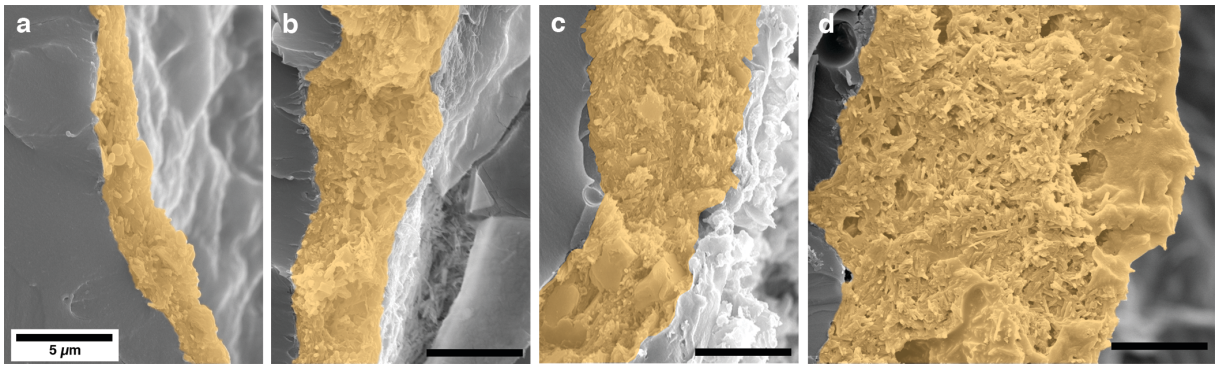


**Figure 2.** SEM imaged microvascular channel longitudinal cross-sections showing matrix-embedded PDADMAC/halloysite reinforcement at a) 10-bilayers, b) 20-bilayers, c) 40-bilayers and d) 80-bilayers. Images are false colored to distinguish multilayers from bulk epoxy.

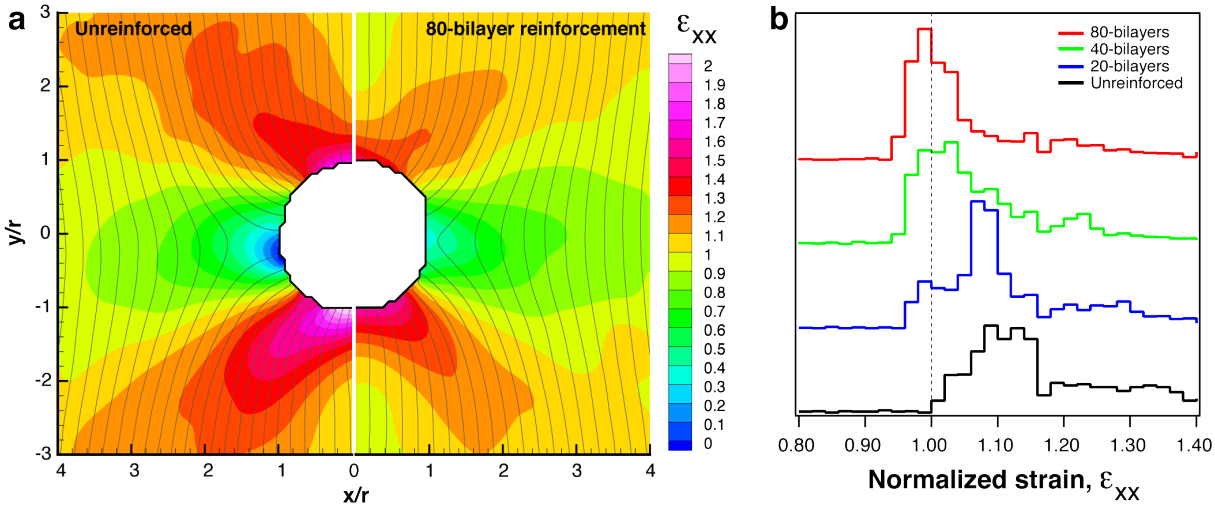


**Figure 3.** a) Normalized strain field as measured by FDIC for an unreinforced (left) and an 80-bilayer PDADMAC/halloysite multilayer-reinforced (right) microvascular channel. b) Histograms of strain measured above and below sample microchannels indicating a reduction in strain for increasing multilayer thickness.

**Halloysite-nanoclay/polycation multilayers** are deposited onto template scaffolds to create oxide-reinforced microvascular networks. Using electrostatic layer-by-layer deposition allows conformal coating of the channel walls with controllable thickness and the presence of halloysite leads to reduced stress concentrations in channel walls under uniaxial tension, and should lead to increased network robustness.

TOC Keyword

C. Author-Two, D. E. F. Author-Three, A. B. Corresponding Author*((same order as byline))■<B>…<B>■

Structural Reinforcement of Microvascular Networks Using Electrostatic Layer-by-Layer Assembly with Halloysite Nanotubes

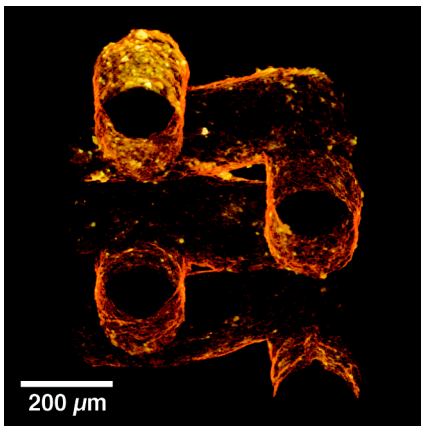

Supporting Information should be included here (for submission only; for **publication**, please provide Supporting Information as a separate PDF file).

**Supporting Information**
All figures and movie filenames are numbered in the order of reference in the main body of the paper.

1.1 "SupFigure1.tif"
SEM image of microvascular channel edge with deposited PDADMAC/halloysite multilayer. EDAX spectra of (a) the epoxy surface and the (b) multilayer show the presence of silicon and aluminium in the multilayer but not in the epoxy.

1.2 "SupFigure2.tif"
Graph of number of deposited PDADMAC/halloysite multilayers vs. multilayer thickness as measured by SEM. Error bars show one standard deviation from the mean. A linear fit to the data yields a value of 188 ± 7 nm per bilayer with a chi-square value of 0.229.

1.3 "SupMovie3.mpg"
Rotating MicroCT reconstruction of a section of microvascular network within an epoxy matrix containing a deposited $(PDADMAC/halloysite)_{80}$ multilayer. Increasing brightness indicates increasing X-ray contrast.

1.4 "SupFigure4.tif"
FDIC measurements (left side) and analytical solutions (right side) of strain fields for channels with 80-bilayer (top) and 40-bilayer (bottom) deposited (PDADMAC/halloysite) films. The film thicknesses used as input for the analytical solutions was taken from SEM measurements, and the modulus used to match FDIC was roughly estimated by direct visual comparison. Note that the analytical solutions show a distinct ring region attributed to the reinforcing film, but this was not visible in the experimental data, perhaps due to the resolution of the technique.